PAPER

Check for updates

Defluorination of borehole water using activated clay and bauxite-laden polyvinyl alcohol hybrid membranes

Andrews Ayim Oduro,[a] Wisdom Selassie Seaneye,[b] Kodwo Miezah,[b] Willliam Wilson Anku[c] and Eric Selorm Agorku [ID] *[a]

Fluoride contamination in drinking water is a major global concern because of its significant health hazards. In many regions in Ghana and some other parts of the globe, fluoride levels rise to high levels, which leads to severe cases of fluorosis and skeletal disorders. Despite improvements in treatment techniques, the necessity of more sustainable and affordable methods and materials to achieve compliance with recommended fluoride limits still remains. Membrane filtration has emerged as a key technique in advanced wastewater treatment, where control of membrane fouling is essential for the feasibility of the process. This study delves into the fabrication and evaluation of activated clay (AC) and bauxite (BXT) incorporated in polyvinyl alcohol (PVA) composite membranes (MPVA/BXT:AC) for mitigating membrane fouling during water defluorination. The physical and chemical characteristics of the membranes were examined using Fourier transform infrared (FTIR) spectroscopy, proton-nuclear magnetic resonance (^{1}H NMR), zeta potential (ZP), X-ray diffraction (XRD), and scanning electron microscopy equipped with EDS. Fluoride removal efficiency and membrane performance were evaluated by conducting water filtration experiments at varying filler concentrations. The results revealed that the MPVA/1BXT:2AC membrane exhibited remarkable fluoride removal efficiency, achieving up to a defluorination rate of 92.4% and a flux recovery rate of 82.6%, indicating its excellent antifouling performance. This membrane had higher porosity and pure water flux (PWF) values of 69.2% and 73.1 L m^{-2} h^{-1}, respectively.

1 Introduction

Water is an important resource for sustaining human life and the environment. Underground water has been the most reliable source in many traditional societies in Ghana, where it is accessed *via* boreholes and non-mechanised well excavation to satisfy the demand for drinking purposes. However, this quality is usually compromised by pollution resulting from a combination of human activities and natural causes.[1] Fluoride is a naturally occurring element found in the Earth's crust, commonly found in rocks, soils, water, and the atmosphere. While some amounts of fluoride may be good for the teeth and bone, prolonged exposure to high concentrations, especially through drinking water, can have serious health implications. The major sources of fluoride contamination are the weathering and leaching of fluoride-bearing minerals such as fluorite, apatite, and mica.[2] Man-made activities such as phosphate fertilizer application, coal burning, ceramics production, and brick manufacture have increased fluoride emissions into the environment.[3] In areas with geothermal activity, fluoride-rich gas and steam also contribute to groundwater contamination. The maximum fluoride content limit set by the World Health Organization (WHO) for drinking water is 1.5 mg L^{-1}, but in arid and semi-arid zones, with groundwater predominating as the water source, this limit is often exceeded.[4] Long-term intake of fluoride-laden drinking water can cause various health issues, ranging from dental and skeletal fluorosis to neurological disorders and gastrointestinal problems, which affect reproduction.[5] Children and pregnant women, in particular, are vulnerable to fluoride exposure.[6]

In Ghana, fluoride pollution is much more prevalent in the northern parts of the country, where many of the communities depend solely on boreholes and wells for their drinking water.[7] Reports have shown levels of fluoride concentrations far above the WHO guidelines in several districts, making fluoride contamination not just an ambient environmental concern but a region-specific public health emergency.[7–10] Because of many of

[a]Department of Chemistry, Kwame Nkrumah University of Science and Technology, PMB, Kumasi, Ghana. E-mail: seaky2k@gmail.com; Tel: +233 549394366
[b]Department of Environmental Science, Kwame Nkrumah University of Science and Technology, PMB, Kumasi, Ghana
[c]Department of Physical and Mathematical Sciences, University of Environment and Sustainable Development, PMB, Somanya, Eastern Region, Ghana

the residents in these areas have been in constant contact with water with high fluoride levels, it has been established that water consumption is highly associated with dental and skeletal fluorosis,[11,12] which thus calls for appropriate, cost-effective and sustainable technologies tailored specifically for these regions in terms of defluorination.

Several methods, such as precipitation, ion exchange, adsorption and electrocoagulation, have been successfully used in treating fluoride-contaminated water. Despite these advancements, there remains a need for more effective and affordable technologies and materials to achieve compliance with the recommended fluoride limits. Adsorption-based membrane filtration offers the greatest promise because of its simplicity in operation and low energy demand, allowing contaminant removal while enhancing membrane performance.[13] However, one major limitation of membrane processes is fouling: the accumulation of organic matter and suspended solids on the membrane surface and within its pores.[14] Fouling results in reduced membrane permeability, increased transmembrane pressure and a shorter life span for the filtration system.

Recent advances in developing hybrid membranes have been targeting better applications by incorporating functional materials into polymeric matrices.[15–17] Polyvinyl alcohol, a hydrophilic, non-toxic and chemically stable polymer, has attracted much attention as an excellent film-forming and robust mechanical material.[18] The innovation of this study emerges in the synthesis of a newly developed PVA-based hybrid membrane embedded with bauxite and activated clay, two naturally available and cost-effective materials with inherent adsorptive properties. Bauxite, a naturally occurring aluminium ore available and mined in Ghana, is rich in alumina with a high surface area and chemical reactivity.[19] This makes it an available, cheap, and feasible material for fluoride adsorption through ion exchange and surface complexation. Activated clay, known for its high porosity, ion exchange ability, and large surface area, enhances the fluoride-binding ability of the membrane while contributing to its antifouling properties.[20]

The synergy between these three materials, PVA, bauxite, and activated clay, provides the foundation for the preparation of dual-functional membranes capable of fluoride removal and fouling resistance. The membrane consists of PVA as the major constituent and serves the function of maintaining an essential hydrophilic environment for membrane stability and water permeation. Bauxite is embedded to provide sites that are highly affinitive to fluoride adsorption, while activated clay enhances the ion-exchange interactions and prevents foulant accumulation due to its surface charge.[21] This composite membrane is an economical and environmentally friendly alternative to conventional membranes, which are usually synthetic or costly materials. Considering the locally available raw materials, the membrane can also be conveniently deployed in fluoride-endemic and resource-limited areas such as Northern Ghana.

This study describes the fabrication of a PVA/bauxite/activated clay composite membrane for the simultaneous removal of fluoride from water and controlling fouling during water treatment. This study also contributes to the vision of safe and sustainable water treatment at the local and global levels, most especially for communities where fluorosis is endemic.

2 Experimental

2.1 Chemicals

Commercial grade polyvinyl alcohol (PVA, with an average molecular weight of 86.09 g mol^{-1}) was purchased from Molychem, India. Sulphuric acid (H_2SO_4, with a purity of >98%), hydrochloric acid (HCl, 37% w/w analytical grade) and sodium hydroxide (NaOH, with a purity of >98%) were purchased from Sigma-Aldrich, USA.

2.2 Method

2.2.1 Clay and bauxite sample collection and preparation. The clay sample, obtained from Teleku Bukazo in Ghana's Western Region, was initially cleaned to remove any foreign materials. It was then compacted into bars using a soil compactor. These bars were cut into smaller sections and left to air dry. The dried clay was ground into a fine powder using a mechanical milling machine. The bauxite (BXT) sample was collected from Atiwa Forest at Kyebi in the Eastern Region of Ghana. It was thoroughly washed thrice with distilled water to remove impurities and foreign materials. The bauxite was air-dried, crushed, and sieved through a micro mesh to ensure particle size consistency.

The raw and fluorinated water was sourced from three boreholes, one each in Daku, Kuseli, and Dabo, all in the Upper West Region, Wa West district (Ghana), into clean 4.5 L gallons. The samples of borehole water were coded as D1 and D2 (Daku), K1 and K2 (Kuseli), and DB1 and DB2 (Dabo). The gallons were tightly sealed and transported to the chemistry laboratory at the Kwame Nkrumah University of Science and Technology (KNUST), where they were securely stored for analysis.

2.2.2 Synthesis of activated clay. A 500 mL beaker was filled with 25 g of measured raw clay and 100 mL of distilled water. Using a magnetic stirrer, the mixture was continuously stirred until a uniform suspension was achieved. The clay suspension was then mixed with 100 mL of 15% concentrated sulphuric acid (H_2SO_4), and the mixture was thoroughly agitated to make sure the acid was evenly distributed. The mixture was left undisturbed overnight. The activated clay was then filtered out. After pH-neutralizing washing with distilled water, it was dried at 70 °C in a hot oven and ground into a fine powder.

2.2.3 Synthesis of MPVA/BXT and MPVA/AC:BXT composite membranes. Using the solution casting approach and distilled water as the solvent, membranes made of MPVA/BXT and MPVA/AC:BXT in different ratios of AC to BXT were synthesized. To prepare a PVA solution, 5 g of PVA was first dissolved in 40 mL of distilled water and continuously agitated with a magnetic stirrer while being refluxed at 90 °C for 4 hours. Table 1 shows the various amounts of AC and BXT fillers that were added. In a separate step, specified amounts of AC and BXT were suspended in 15 mL of distilled water. The PVA solution was then mixed with this solution and subjected

Table 1 Composition of MPVA/BXT and MPVA/BXT:AC membranes

Membrane	PVA (wt%)	BXT (wt%)	AC (wt%)
MPVA/1BXT	4.0	2.0	—
MPVA/3BXT	4.0	4.0	—
MPVA/6BXT	4.0	6.0	—
MPVA/1BXT:1AC	5	2.5	2.5
MPVA/1BXT:2AC	5	1.6	3.4
MPVA/2BXT:1AC	5	3.4	1.6

to ultrasonic processing for one hour. The combined solutions were then subjected to an additional hour of sonication. To create uniform membranes, the resulting solutions were cast on previously cleaned glass plates. For five (5) days, these membranes were allowed to air dry.

2.3 Characterization techniques

The functional groups of MPVA/BXT:AC composite membranes were determined by employing Fourier transform infrared spectroscopy (FTIR: Model: BRUKER ALPHA PLATINUM ATR-FTIR; Germany), while structural analysis was performed on the composite membranes by proton-nuclear magnetic resonance (^{1}H NMR). The particle size and zeta potential of the MPVA/1BXT:2AC composite membrane were measured using a Zetasizer (Model: Malvern PANalytical, UK). The ZP of particles was measured to determine the polydispersity index (PDI), which identifies the uniformity of particle size distribution. Moreover, it also provides information regarding the surface charge and stability of colloidal systems. The mineralogical composition of PVA, activated clay, bauxite, and MPVA/BXT:AC composite membranes was studied by X-ray diffraction analysis (Shimadzu XRD-7000, Japan) using Cu-Kα X-ray radiation (λ = 1.5418 Å). The membranes' surface morphology and elemental compositions were analyzed using a Zeiss EVO MA 15 SEM-EDX (Germany). An ion-selective electrode (ISE) fluoride analyser from HANNA Instruments (Tokyo, Japan) was used to analyze fluoride concentrations in the samples before and after filtration.[4]

2.4 Pure water flux and fluoride elimination

A dead-end membrane unit was utilized to analyze the pure water flux of various membranes fabricated with an area of 77.5 cm^2.[22] The pure water flux (PWF) of the membranes was measured under a pressure of 12 MPa. Measurement of the pure water flux (J_0), sample water (V), and permeate flux (J_2) was made every 10 minutes at room temperature under constant pressure for 60 minutes at 5 bar. To account for reversible fouling due to fluoride adsorption, membranes were first cleaned with a diluted hydrochloric acid (HCl) solution before rinsing with distilled water.[23] The permeate flux (J_p) was determined according to eqn (1).[24]

$$\text{Flux } (J_p) = \frac{V}{A\Delta T} \qquad (1)$$

where V is the permeate volume in litres (L), J_p is the permeate water flux (L m^{-2} h^{-1}), t is the filtration time in hours (h), and A is the membrane surface area in square meters (m^2).

To study the effects of the feed solution on separation performance, the membrane performance was evaluated with the sampled water. Using eqn (2),[25] the fluoride removal efficiency was determined.

$$\text{Removal efficiency (RE)}(\%) = \left(\frac{C_F - C_P}{C_F}\right) \times 100 \qquad (2)$$

where C_P and C_F correspond to the fluoride levels in the feed and the permeate, respectively. The flux recovery rate (FRR%) was determined from eqn (3).[24]

$$\text{FFR }(\%) = \frac{Q_2}{Q_0} \times 100\% \qquad (3)$$

where Q_0 is the flux after the membrane is washed with dilute HCl in (L m^{-2} h^{-1}) and Q_2 is the pure water flux (PWF) in (L m^{-2} h^{-1}).

2.5 Porosity

The measurements of wet and dry membrane weight loss were examined to assess the porosity of the membranes.[26] The membranes were cut to size and then measured. The membranes were weighed and then submerged in distilled water for 24 hours to completely saturate the membranes by allowing the distilled water to infiltrate and fill the pores. The weight of the wet membrane was determined first and then the dry membrane. Each membrane was tested for porosity (P). The determination of the porosity of the membranes was calculated using eqn (4).[25]

$$P(\%) = \frac{Q_1 - Q_0}{Ah} \times 100\% \qquad (4)$$

where the membrane area A is in square meters (m^2), h is the thickness of the membrane in micrometres (μm), and Q_0 is the weight of the dry membrane in grams. The mass of the wet membrane is Q_1 in grams.

2.6 Anti-fouling performance

The flux recovery ratio (FRR) is inversely proportional to membrane fouling. Fouling of membranes, a common problem, occurs when molecules adhere to the surface and pores of the membrane. The fouling of the membrane was calculated using eqn (5).[25]

$$\text{Fouling }(\%) = 1 - \frac{Q_2}{Q_0} \times 100\% \qquad (5)$$

2.7 Membrane reusability

The reusability test of the best-performing membrane (MPVA/1BXT:2AC) was performed through four filtration cycles. Before each reuse cycle for the membrane, it was cleaned using dilute HCl, followed by rinsing with distilled water.[27]

3 Results and discussion

Recent advancements in membrane technology have brought about the vital importance of understanding material charac-

terization in improving membrane functionality for a wide array of applications. Characterization techniques such as Fourier transform infrared (FTIR) spectroscopy, X-ray diffraction (XRD), scanning electron microscopy (SEM)/energy dispersive X-ray spectroscopy (EDS), zeta potential (ZP) and nuclear magnetic resonance (NMR) provide valuable insights into the structural, morphological, and elemental compositions and surface and chemical features of the membrane materials.

3.1 FTIR analysis

The FTIR spectra of activated clay (AC), bauxite (BXT), polyvinyl alcohol (PVA), MPVA/BXT:AC and MPVA/BXT are displayed in Fig. 1. Fig. 1a shows vibrational patterns in AC, notably at 1035, 911, 778, and 529 cm^{-1}, which reflect the presence of distinct functional groups that include the OH deformation, SiO_2, Si–OH, and Al–O, respectively.[28] The FTIR spectrum for bauxite indicates a strong OH stretching peak at 3400 cm^{-1},

which signifies hydroxyl existence from gibbsite ($Al(OH)_3$), a main component in bauxite.[29] Additionally, peaks at 1100 cm^{-1} and 956 cm^{-1} validate Si–O and AlOH occurrence, respectively.[30] A peak at 550 cm^{-1}, which is related to the stretching vibrations of Fe–O, attests to the presence of iron oxides in bauxite and indicates its mineralogical composition. Hydroxyl (OH) groups involved in hydrogen bonding exhibit a pronounced peak at 3265 cm^{-1} in PVA. The peak at 2910 cm^{-1} is indicative of aliphatic vibrations, and the peak at 1709 cm^{-1} reveals the carbonyl (C=O) stretch.[31] In addition, the peak at 1419 cm^{-1} indicates C–H bending vibrations. The peak at 1082 cm^{-1} represents the stretching vibrations of the C–O bond in ether groups, and the peak at 834 cm^{-1} corresponds to the C–C–O group stretching vibrations in PVA.[30]

In Fig. 1b, the analysis continues with the spectrum of the MPVA/BXT:AC composite, where the evidence of strong interactions due to the incorporation of bauxite and activated clay
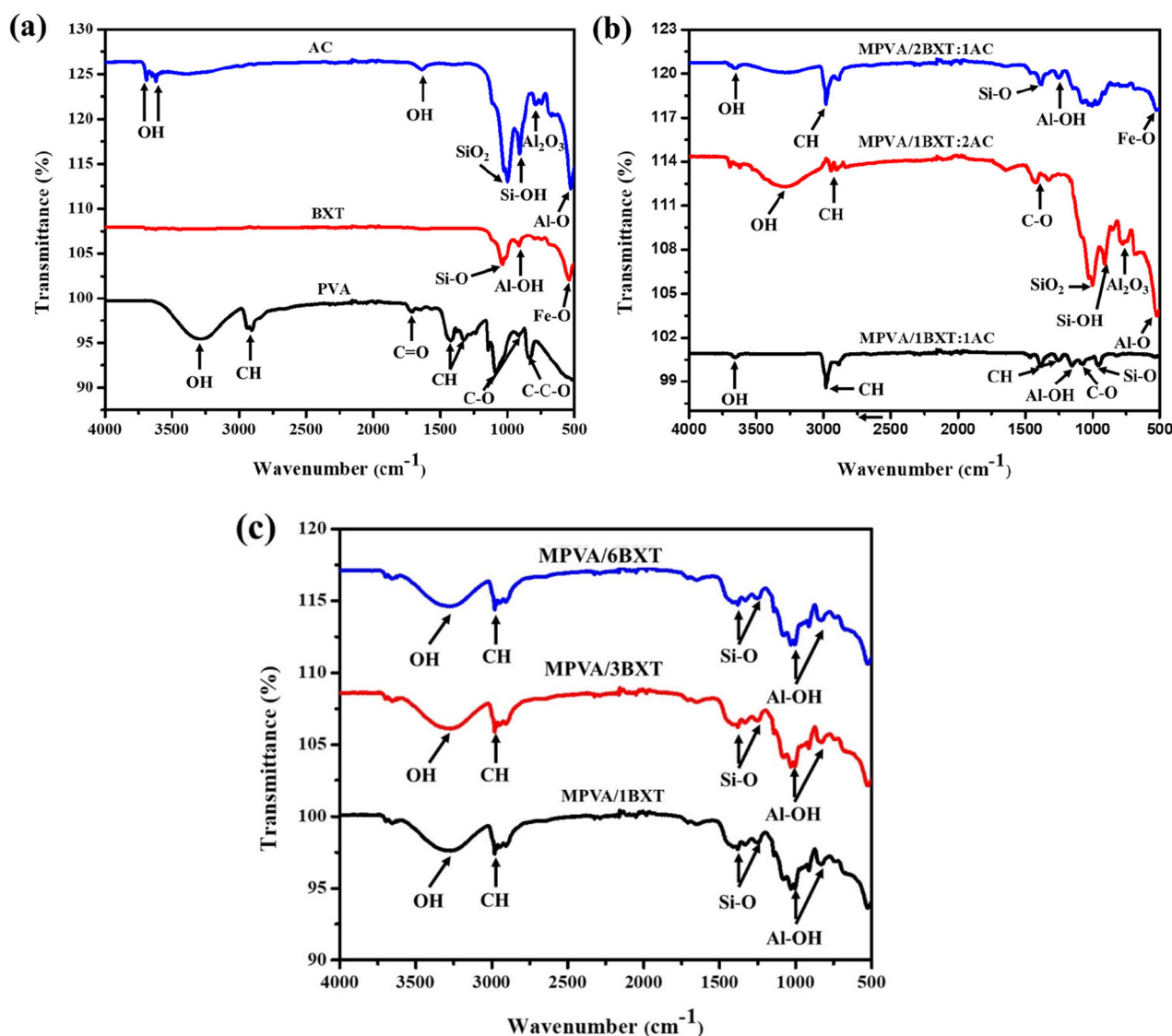

Fig. 1 FTIR spectra of (a) AC, BXT and PVA, and (b) MPVA/BXT:AC and (c) MPVA/BXT composite membranes.

prevails in the presence of the OH stretching peak at 3400 cm^1. The C–H stretching peak at 2900 cm^{-1} persists, indicative of the PVA matrix. An indication of the successful migration of silicate structures from activated clay to the polymer matrix is shown by the Si–O stretching peak at 1000 cm^{-1}. Peaks at 876 cm^{-1}, 675 cm^{-1} and 560 cm^{-1} indicate Si–OH, Al_2O_3, and Al–O groups in the AC, respectively.[32] The retention of the Fe–O stretching peak at 550 cm^{-1} confirms that iron oxides from bauxite are being retained within the composite.

The influence of the variation of the AC content on the MPVA/bauxite composite is presented in Fig. 1c. The MPVA/1BXT composite spectrum reveals a broad OH stretching at 3400 cm^{-1}, thus confirming substantial hydrogen bonding interactions between the PVA matrix and AC. The C–H stretching peak at 2900 cm^{-1} and the Si–O stretching peak at 1000 cm^{-1} remain fairly strong, confirming again the presence of AC in the PVA matrix. Evidence for aluminium hydroxides is observed at the 900 cm^{-1} peak (Al-OH bending), which could potentially affect the mechanical properties of the materials. In the case of the MPVA/3BXT composite, the observed intensity of the OH stretching peak at 3400 cm^{-1} is reduced, indicating a lower clay content and lesser interaction than in the case of the 6% formulation. PVA is integrated into bauxite at a lower interaction level, as evidenced by other peaks, such as the C–H stretching at 2900 cm^{-1} and the Si–O stretching at 1000 cm^{-1}.[33] In contrast, the spectrum of the MPVA/6BXT composite shows a higher intensity of the OH stretching peak at 3400 cm^{-1}, suggesting that the presence of the increased clay content led to enhanced hydrogen bonding interactions. This is further supported by the more pronounced Si–O stretching peak at 1000 cm^{-1}, indicating a considerable AC contribution to the composite structure.

3.2 XRD analysis

The diffractograms illustrated in Fig. 2a and b show the characteristic features of polyvinyl alcohol (PVA), bauxite (BXT), and activated clay (AC) composites in terms of their crystallinity and phase behaviour. The XRD pattern of pristine MPVA manifests in Fig. 2a with the evidence of a broad peak centred at 19.5°, which substantiates its semi-crystalline nature. This peak indicates that crystalline regions may exist within the amorphous matrix of PVA, a behaviour seen in many polymer systems.[34] With the addition of bauxite into the MPVA matrix, there is a significant increase in peak intensity at around 29.5°. This improvement is associated with the characteristic peaks of bauxite, due to the presence of gibbsite mineral ($Al(OH)_3$) and firm confirmation from the additional peaks at 20.5° and 30.5°.[35] The presence of these peaks, together with the polymer system, has proven that bauxite was incorporated successfully, indicating that strong interactions between PVA and mineral fillers were established. Composites with varying contents of bauxite were studied (MPVA/1BXT, MPVA/3BXT, and MPVA/6BXT). The higher the amount of bauxite, the higher the corresponding intensity of the peaks, particularly at 29.5°. The highest peak intensity can be seen

Fig. 2 XRD diffractograms of (a) MPVA, BXT and MPVA/BXT membranes, and (b) AC and MPVA/BXT:AC composite membranes.

within the MPVA/6BXT composite, which shows an effective polymer interaction with the mineral filler and suggests an enhanced crystalline order. These findings are in agreement with previous studies, which reported that increased filler content can improve crystallinity and mechanical properties in polymer composites, possibly due to improved load transfer and polymer–filler interactions.[36]

In Fig. 2b, the diffractograms show AC and its composites with PVA and bauxite and give more insights into the structural behaviour of these materials. The AC shows distinct peaks at 15.5° and 28.5°, which attest to its crystalline nature, mainly due to the presence of montmorillonite. When AC and BXT are incorporated in PVA, as seen in the patterns for MPVA/1BXT:1AC, MPVA/1BXT:2AC, and MPVA/2BXT:1AC, enormous variations in the diffractograms were observed. The peaks at 29.5° and 20.5° indicate the successful incorporation of bauxite into the PVA matrix. The intensity of the peak associated with AC gradually decreases in these composite formulations, which indicates that the polymer matrix may affect the clay's crystalline behaviour, possibly due to polymer chain entanglements or interaction effects. A noticeable shift in the peak intensity and position in the MPVA/1BXT:2AC composite membrane reveals a modification in the crystalline structure due to the interaction between the components. This observation is consistent with previous investigations, which states that the decrease in peak intensity correlates with increased polymer–filler interaction, leading to less crystallinity in filler materials.[37]

3.3 ^{1}H NMR of MPVA and the MPVA/1BXT:2AC composite membrane

The structural integrity and molecular interaction within the MPVA matrix, as well as that of the MPVA/1BXT:2AC composite membrane, were studied using the ^{1}H NMR spectroscopic technique with D_2O as a solvent. Fig. 3 shows the spectra of MPVA and the MPVA/1BXT:2AC composite membrane.

In the MPVA spectrum (Fig. 3a), two peaks characteristic of proton resonances were observed: a broad one at around 1.3 to 1.6 ppm, which corresponds to methylene ($-CH_2-$) backbone protons, and another broad one at approximately 3.8 to 4.2 ppm, attributed to methine ($-CH-OH$) protons bonded next to hydroxyl groups.[38,39] As expected, in D_2O, the exchangeable hydroxyl protons were not observed because they have undergone rapid deuterium exchange with the solvent.

The MPVA/1BXT:2AC composite membrane retained the characteristic PVA signals, showing that the polymer main chain was not chemically altered during blending (Fig. 3b). However, the methine proton signal centred at 3.8 to 4.2 ppm showed slight broadening and possibly shifted downfield with respect to the MPVA spectrum. This broadening comes from the restricted molecular mobility of the polymer chains upon the incorporation of the inorganic components and the possible formation of intermolecular interactions (*e.g.*, hydrogen bonding, coordination) between PVA hydroxyl groups and metal sites (Al^{3+}, Fe^{3+}) on the bauxite and activated clay surfaces.[40]

The observed chemical shift changes and increased broadness in the composite spectrum point toward a successful integration of the inorganic fillers into the PVA matrix. This indicates close contact between the polymer and filler phases, which contributes to interfacial compatibility, mechanical integrity, and functional performance of the membrane. The retention of the PVA backbone and the successful dispersion and interaction of the inorganic fillers within the PVA matrix confirm their structural role in the composite membrane.
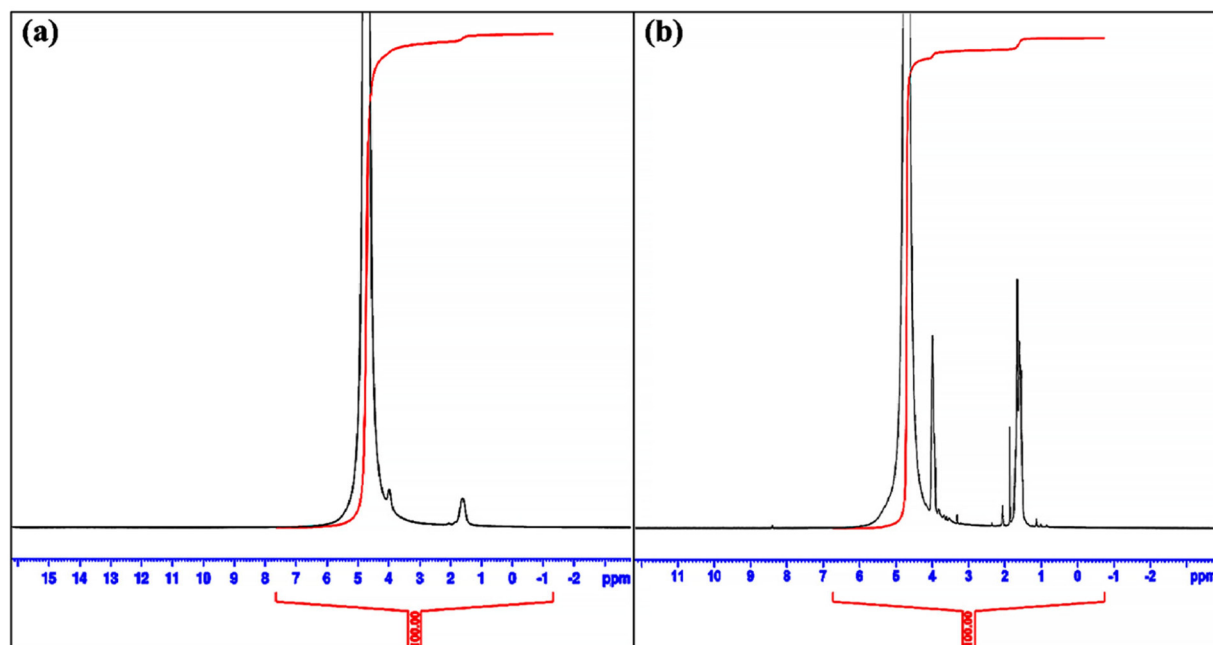

Fig. 3 ^{1}H NMR spectrum of (a) pure PVA and (b) the MPVA/1BXT:2AC composite membrane.

3.4 SEM analysis of the MPVA/1BXT:2AC membrane

The membrane surface showed an amorphous structure with an apparent interaction among the three components, PVA, BXT, and AC (Fig. 4). The primary structure of the membrane was shown to consist of the PVA matrix, which at a lower imaging magnification also shows a web-like structure of PVA strands, indicating a well-integrated system. The PVA matrix is uniform, which enables the anchoring of other materials. The surface of the membrane is evenly distributed with AC fine powder, which is well dispersed except for a few agglomerates and clusters. The surface roughness brought by the incorporation of AC may affect properties such as enhanced mechanical strength and improved adsorption.[41] Bauxite particles can be seen in the matrix on the surface, mostly adjacent to the clusters of AC particles, which contribute to the textural quality of the surface. There are signs of clear synergism between BXT and PVA, which can be characterized as affecting the surface characteristics of the membrane. The presence of BXT and AC aids in the formation of pores within the membrane, resulting in increased permeability of the membrane. The inclusion of activated clay and bauxite into the PVA matrix had a strong influence on the membrane morphology, leading to the development of micropores and mesopores on the membranes. These fillers disrupted the dense polymer matrix, thus forming voids that promote water permeability and provide active sites for adsorption. Porosity analysis revealed that MPVA/1BXT:2AC had a porosity of 69.2%, indicating a high void fraction favourable for mass transport through the membrane. These porous structures aid in flux enhancement while reducing membrane fouling *via* size exclusion and adsorption mechanisms. MPVA/1BXT:2AC shows a well-developed pore structure with a large surface area, micro to mesopores and interconnected voids.

3.5 EDX analysis of the MPVA/1BXT:2AC membrane

The EDX analysis (Fig. 5) shows the elemental composition and weight percentage of the constituents. The most abundant element is oxygen, which is present in PVA, BXT and AC minerals and accounts for 45.27%, indicating that the composite membrane is hydrophilic. The carbon content, which is the second most abundant among all elements at 33.20%, is due to the PVA component of the membrane. Silicon (6.68%), calcium (1.08%), iron (0.96%), magnesium (0.22%), sodium (4.43%) and aluminium (1.08%) were all present in trace amounts, which indicates the presence of AC and BXT minerals like quartz and albite in the structure of the membrane.[42] The presence of sulphur (2.74%) suggests that there may be interactions between the clay and the acid during the process of clay activation, and it may also be part of AC and BXT.

3.6 Zeta potential of the MPVA/1BXT:2AC membrane

The zeta potential (ZP) serves as a key measure of material surface charge, porosity, and filtration efficiency.[43] Fig. 6 illustrates the particle size distribution by volume (a), size distribution by intensity (b), and zeta potential distribution (c) for the MPVA/1BXT:2AC composite membrane. Both the size distributions by intensity and volume show that the MPVA/1BXT:2AC composite membrane has an average zeta diameter of 885.2 nm, a zeta potential of −1.27 mV, and a zeta deviation of 149.9 mV. The composite membrane demonstrates a negative zeta potential (−1.27 mV), indicating a negatively charged surface. The negative charge indicates the membrane stability
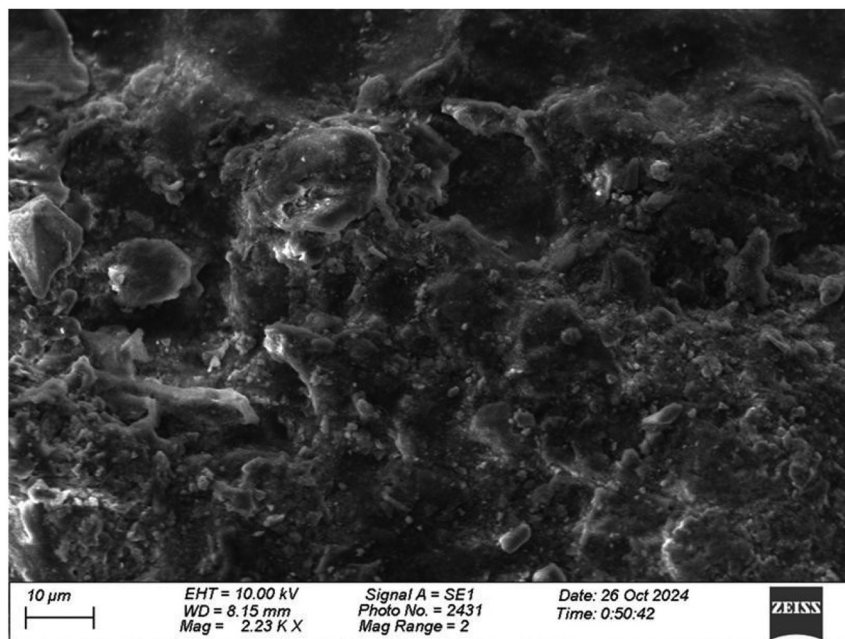

Fig. 4 SEM image of the MPVA/1BXT:2AC composite membrane.
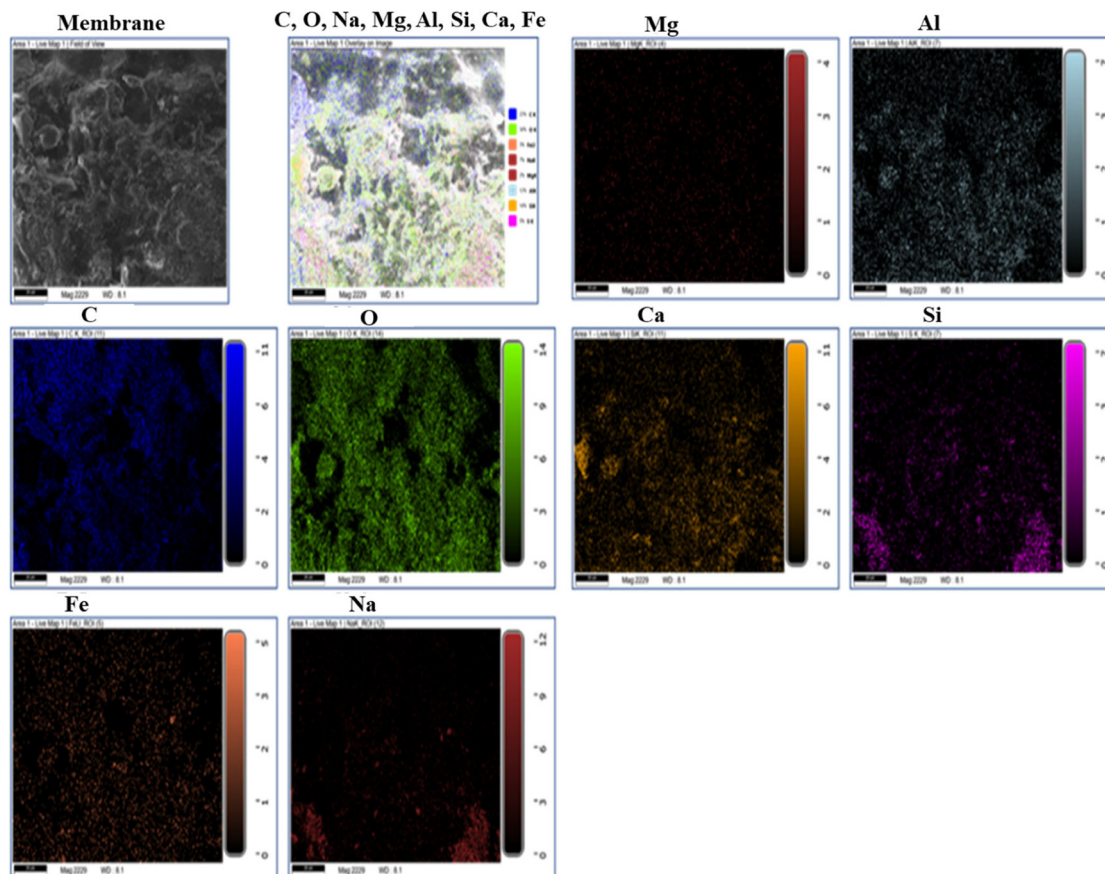
Fig. 5 Elemental mapping of the MPVA/1BXT:2AC composite membrane.

in terms of reduced particle aggregation and the level of electrostatic repulsion existing among similarly charged particles in the dispersion.[44] The negative zeta potential enhances the membrane repulsion against fluoride ions through electrostatic repulsion, which, in effect, aids in fouling mitigation. Thus, it reduces fluoride ion interaction with the membrane surface and improves the transport of fluoride ions towards the adsorption sites within the membrane structure.[45] However, repulsion alone may have little effect on fluoride removal.

Fluoride ions interact with the membrane surface through chemical or physical adsorption and ion exchange mechanisms due to the fillers incorporated, where the fillers show a high ion exchange for fluoride ions, resulting in selective adsorption even when electrostatic repulsion occurs.[46] The negative ZP enhances the membrane's performance by preventing excess ions from accumulating on the membrane surface, thus ensuring maximal adsorption capacity and optimal membrane permeability. The negative ZP indirectly contributes to fluoride removal by reducing fouling and maintaining ion flow while enabling efficient interactions with the fillers. The fluoride is less likely to adhere to the membrane surface unless the applied suction pressure overcomes the repulsive forces. When the membrane dries, these ions can

lodge within the pores, but upon re-wetting, a greater quantity of fluoride dissolves into the water, improving membrane reusability.[47]

Zeta potential and particle size distribution offer crucial insights into the physicochemical properties of membranes. The heterogeneity of the membrane structure is evident from the zeta deviation of 149.9 mV, which may enhance overall performance by improving flow, reducing fouling, increasing porosity, and limiting scaling.[48]

3.7 Membrane performance

An essential component of water filtration, separation, and treatment procedures is membrane efficiency. Porosity, surface configuration, hydrophilicity, pure water flux, and fouling resistance all have an impact on selective transport through the membrane, which is the primary factor. Both selectivity and the rate of transporting materials through the membrane will determine membrane efficiency and application.

3.7.1 Porosity and pure water flux (PWF) of synthesized membranes. Membranes were successfully synthesized, as illustrated in Fig. 7. The porosity and pure water flux (PWF) values for these membranes are presented in Table 2. The results highlight the influence of bauxite as an additive on the structural and transport characteristics of the membranes.
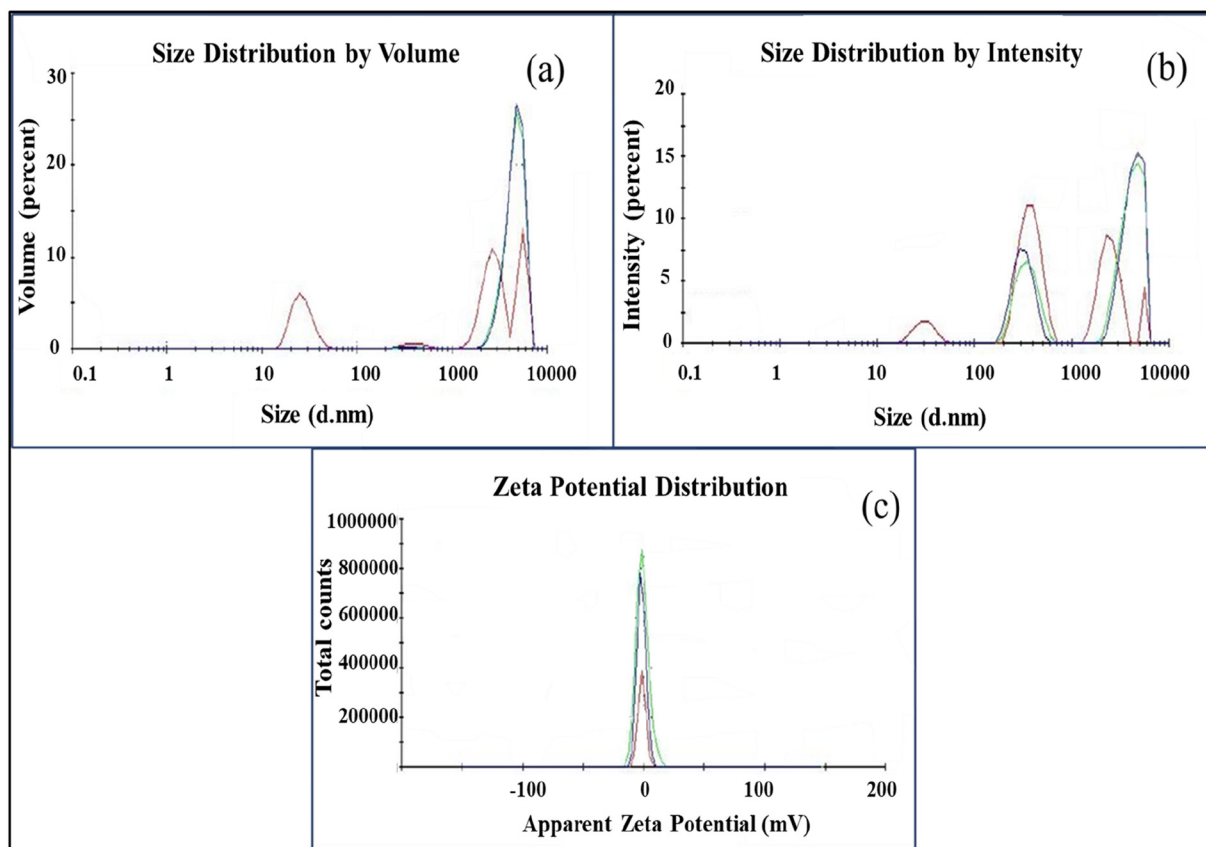
1620 | *RSC Appl. Polym.*, 2025, **3**, 1613–1628

© 2025 The Author(s). Published by the Royal Society of Chemistry

Fig. 6 (a) Size distribution by volume, (b) size distribution by intensity and (c) zeta potential distribution of the MPVA/1BXT:2AC composite membrane.

Fig. 7 Synthesized (a) MPVA/1BXT, (b) MPVA/3BXT and (c) MPVA/6BXT membranes.

Table 2 PWF and porosity of the synthesized membranes

Membrane	Porosity (%)	Pure water flux (L m^{-2} h^{-1})
MPVA/1BXT	49.3	53.5
MPVA/3BXT	56.5	60.1
MPVA/6BXT	57.8	66.9
MPVA/1BXT:1AC	62.1	65.8
MPVA/1BXT:2AC	69.2	73.1
MPVA/2BXT:1AC	58.4	61.7

In Fig. 8, the MPVA/1BXT membrane demonstrated moderate levels of porosity and a PWF value of 53.5 L m^{-2} h^{-1}, with a porosity of 49.3%. In the MPVA:3BXT membrane, there was a notable enhancement in both the porosity and PWF, resulting in values of 56.5% and 60.1 L m^{-2} h^{-1}, respectively. The porous nature of BXT contributes to the development of additional voids within the membrane structure, facilitating improved water permeability. This finding meets expectations, affirming the hypothesis of increased water permeability due

Fig. 8 PWF and porosity of the MPVA/BXT composite membrane.

Fig. 10 Pure water flux and porosity of the MPVA/BXT:AC composite membrane.

to the addition of BXT. The membrane of MPVA/6BXT yielded a porosity of 57.8% and a PWF of 66.9 L m^{-2} h^{-1}. Although these values indicate only a slight increase in porosity and PWF compared to the other membranes, this suggests that increased addition of BXT can enhance membrane characteristics.

A significant correlation emerged from the analysis of the experimental data, as illustrated in Fig. 10, which shows a direct relationship between the porosity of the composite membranes (Fig. 9) and the flux of pure water. The MPVA/1BXT:2AC had the highest PWF (73.1 L m^{-2} h^{-1}) and the greatest porosity (69.2%). This implies that the membrane's structure is more porous and suitable for water mobility. For MPVA/1BXT:1AC and MPVA/2BXT:1AC, on the other hand, the PWF and porosity gradually dropped to 65.8 L m^{-2} h^{-1} (62.1% porosity) and 61.7 L m^{-2} h^{-1} (58.4% porosity), respectively.

3.7.2 Fluoride removal efficiency and antifouling properties. The incorporation of BXT as a filler in the PVA matrix resulted in an improvement in PWF and removal efficiency (RE). Specifically, the MPVA/1BXT membrane exhibited a PWF of 53.5 L m^{-2} h^{-1} and an RE of 56.4%, while the MPVA/3BXT membrane demonstrated a PWF of 60.1 L m^{-2} h^{-1} and an RE of 62.8% (Table 3). The highest performance was observed

Table 3 Pure water flux and removal efficiency of the synthesized membranes

Membrane	Pure water flux (L m^{-2} h^{-1})	RE (%)
MPVA/1BXT	53.5	60.4
MPVA/3BXT	60.1	66.8
MPVA/6BXT	66.9	72.7
MPVA/1BXT:1AC	65.8	84.2
MPVA/1BXT:2AC	73.1	92.4
MPVA/2BXT:1AC	61.7	81.5

with the MPVA/6BXT membrane with a PWF of 66.9 L m^{-2} h^{-1} and an RE of 68.7% (Fig. 11). The enhancement can be attributed to the porous nature of BXT, which improves the membrane structure with more pathways for directly transporting water with consequently greater water flux. Furthermore, the large surface area and adsorption properties of BXT promote enhanced removal efficiency by effectively capturing fluoride ions.

Fig. 12 depicts data for the MPVA/1BXT:1AC membrane with 2.5 wt% of BXT and AC. This membrane achieved a pure

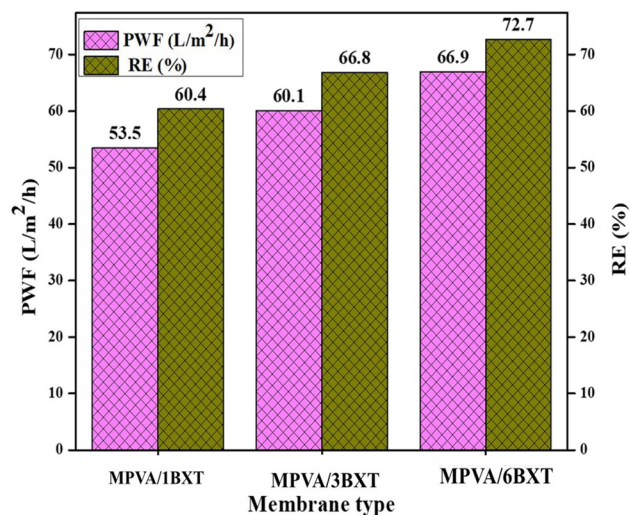**Fig. 9** Synthesized (a) MPVA/1BXT:1AC, (b) MPVA/1BXT:2AC and (c) MPVA/2BXT:1AC membranes.

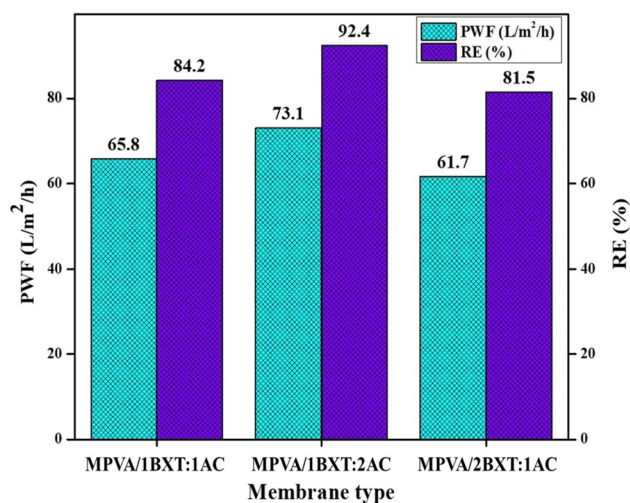**Fig. 11** PWF and RE of the MPVA/BXT composite membrane.

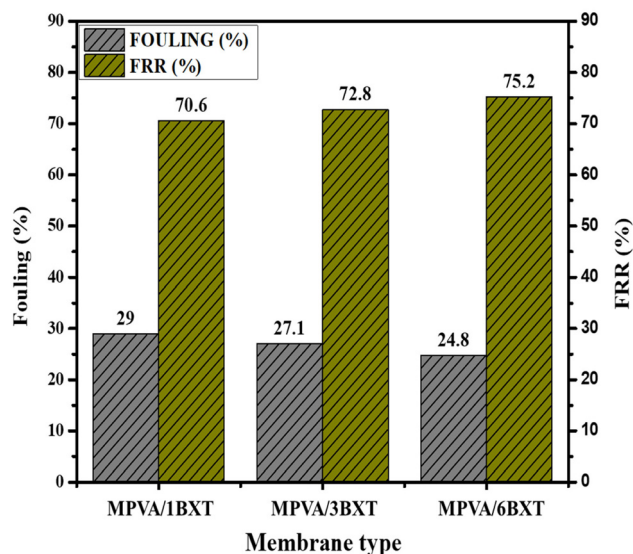**Fig. 12** PWF and RE of the MPVA/BXT:AC composite membrane.

Fig. 13 Fouling and FRR of the MPVA/BXT composite membrane.

Fig. 13 illustrates that the MPVA/1BXT membrane experiences the highest level of fouling (29.0%) and the lowest flux recovery of 70.6%. However, PVA/3BXT resulted in improved filtration efficiency, a higher flux recovery ratio of 72.8% and a low fouling of 27.1%. Similarly, the MPVA/6BXT membrane shows potential as a fouling-resistant material, as demonstrated by its improved performance with an FRR of 75.2% and a fouling rate of 24.8%.

Fig. 14 illustrates how fouling and the flux recovery ratio (FRR) are affected by different filler concentrations. The MPVA/1BXT:2AC membrane exhibited the best flux recovery ratio of 82.6% and the lowest fouling percentage of 17.4% with 1.6 wt% BXT and 3.4 wt% AC. There were noticeable variations in the concentrations of BXT and AC, where AC decreased from
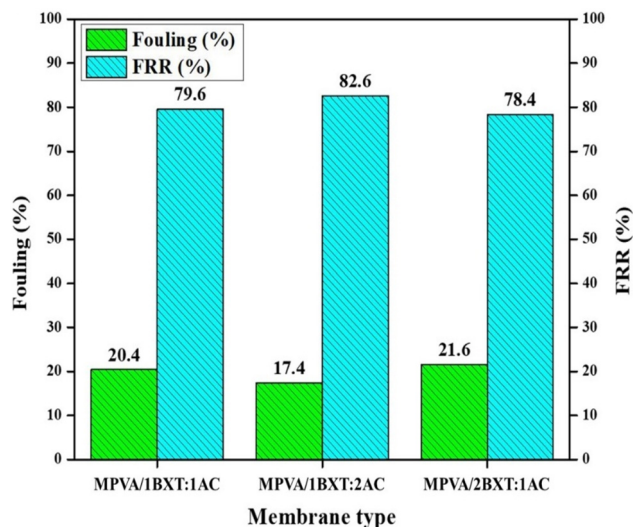
water flux (PWF) of 65.8 L m^{-2} h^{-1} and a removal efficiency (RE) of 84.2%. In contrast, the MPVA/1BXT:2AC membrane exhibited significantly higher PWF and RE values, reaching 73.1 L m^{-2} h^{-1} and 92.4%, respectively. Decreasing the AC content while increasing the BXT content in MPVA/2BXT:1AC resulted in a PWF of 61.7 L m^{-2} h^{-1} and an RE of 81.5% (Table 3).

3.7.3 The fouling behaviour. The enhanced antifouling properties and cleaning efficacy of the composite membranes were evaluated in this study. By observing the flux decrease while filtering 5 mg L^{-1} fluorinated water, the fouling agent, the fouling impact, was ascertained. Following membrane cleaning with dilute HCl and rinsing with distilled water, followed by a filtration procedure to assess flux recovery, a significant decrease in membrane flux was noted when the fluorinated water was substituted with pure water (Fig. 13).

Fig. 14 Fouling and FRR of the MPVA/BXT:AC composite membrane.

Table 4 Reusability of the membrane

PWF (L m^{-2} h^{-1}) before filtration	PWF (L m^{-2} h^{-1}) of fluorinated water	PWF (L m^{-2} h^{-1}) after the first cleaning	PWF (L m^{-2} h^{-1}) after the second cleaning
73.1	69.3	65.8	63.2

3.4 wt% to 1.6 wt% and BXT increased from 1.6 wt% to 3.4 wt%. An FRR of 78.4% and a fouling rate of 21.6% were the outcomes of a decrease in AC content and an increase in BXT concentration. Maintaining both BXT and AC at 2.5 wt% reduced the fouling rate to 20.4% with a FRR of 79.6% (Table 4).

3.8 Fluoride analysis

Raw water samples showed initial fluoride concentrations of 0.40 (D1) and 0.43 (D2) mg L^{-1} from the Daku borehole, 0.47 (K1) and 0.51 (K2) mg L^{-1} from the Kuseli borehole, and 0.54 (DB1) and 0.56 (DB2) mg L^{-1} from the Dabo borehole (Fig. 15). These values are considerably lower than the WHO and Ghanaian standard limit of 1.50 mg L^{-1}.

The MPVA/1BXT membrane decreased the values of fluoride from 0.40 mg L^{-1} to 0.34 mg L^{-1}. This suggests that at this lower value, the bauxite may not be very effective in adsorption. With the MPVA/2BXT:1AC and MPVA/2BXT membranes, the values of fluoride levels fall a little lower from 0.40 mg L^{-1} to 0.30 mg L^{-1} and 0.27 mg L^{-1}, respectively. This implies that AC further increases the efficacy of fluoride rejection with its increasing dose; however, the removal effectiveness is still quite low at these doses. The most significant reduction of the fluoride concentration is observed in the case of MPVA/

1BXT:2AC where the level reaches 0.11 mg L^{-1} from 0.40 mg L^{-1}. This is the minimum fluoride concentration achieved in all the samples and implies that MPVA/1BXT:2AC could be the best membrane for fluoride removal from the water. The application of MPVA/3BXT gave a slight increase in fluoride concentration up to 0.22 mg L^{-1}, which remains lower than the raw water concentration of 0.40 mg L^{-1} but is higher than the concentration that was attained using MPVA/1BXT:2AC. MPVA/6BXT reduced the fluoride level from 0.40 mg L^{-1} to 0.20 mg L^{-1}, suggesting that increasing the concentration of BXT further may not yield a corresponding increase in the removal of fluoride. This shows that there might be a maximum level beyond which adding more BXT does not result in much fluoride sorption.

The study indicates that bauxite and activated clay are effective in removing fluoride ions, yet their usefulness varies with the amount used. Maximum fluoride uptake was recorded for MPVA/1BXT:2AC, with a decrease in fluoride levels from 0.40 mg L^{-1} to 0.11 mg L^{-1}, the least achieved in the study (Fig. 16). These findings suggest that both bauxite and activated clay can also function as effective adsorbent materials for removing fluoride ions.

The MPVA/1BXT:2AC membrane demonstrated consistency in reducing the fluoride levels between 0.11 and 0.12 mg L^{-1}

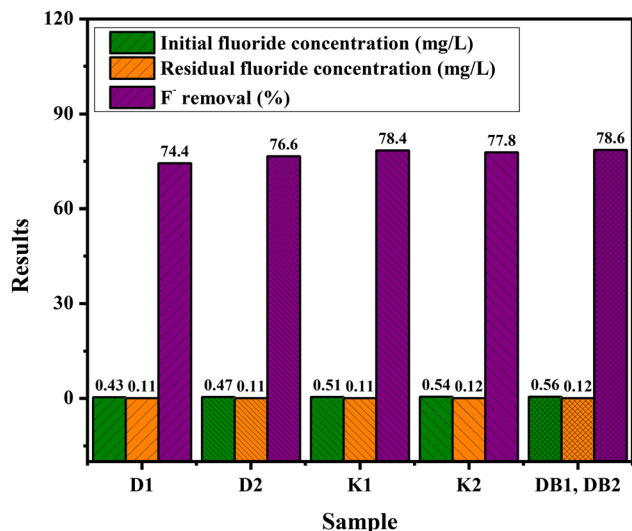**Fig. 15** Water quality analysis in the Dako borehole (D1 and D2).

Fig. 16 Water quality analysis of MPVA/1BXT:2AC in Dako, Kuseli and Dabo boreholes.

(fig. 16). Significantly, this performance was marked when the initial concentration was higher (0.56 mg L^{-1}). This translates to the post-treatment fluoride levels going down significantly.[49] The membrane's optimized composition with a 1 : 2
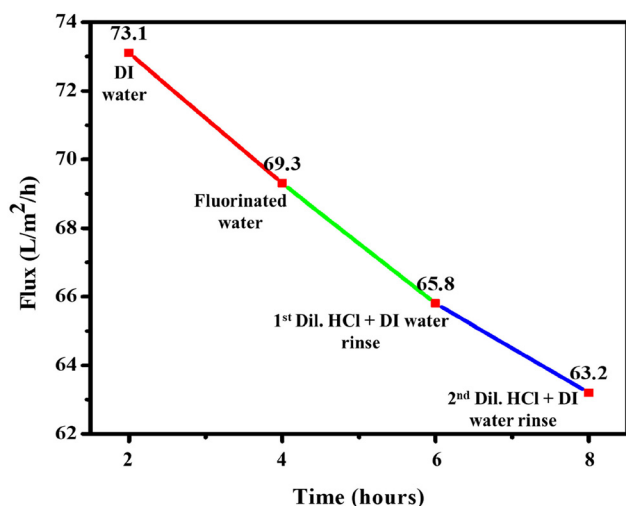

Fig. 17 Longevity performance of the MPVA/1BXT:2AC composite membrane.

ratio of bauxite to activated clay in MPVA provides an ideal balance of adsorption capacity and synergistic effects.

3.9 Reusability and longevity assessment

To assess the longevity performance of the best-performing membrane (MPVA/1BXT:2AC), four consecutive filtration cycles were performed. As shown in Fig. 17 and listed in Table 4, during the first cycle, the membrane showed an initial water flux of 73.1 L m^{-2} h^{-1}. The second cycle showed a slightly lower flux of 69.3 L m^{-2} h^{-1} after being subjected to fluorinated water, indicating a low degree of fouling from the accumulation of fluoride ions. The water flux rate was 65.8 L m^{-2} h^{-1} during the third operation cycle of membrane regeneration after a 30-minute procedure involving a dilute HCl rinse, followed by distilled water. In the fourth cycle, after a repeated cleaning step, the flux was maintained at 63.2 L m^{-2} h^{-1}, implying a slight decline and consistent recovery performance. This great recovery is evidence that surface-bound contaminants were efficiently removed during cleaning, rendering the membrane functional again for multiple operational cycles. The results prove the mechanical stability of the membrane and strong resistance against performance degradation upon repeated use. Table 5 shows a comparison of our membrane's efficiency to other membranes.

3.10 Proposed mechanism of fluoride removal by the MPVA/BXT/AC composite membrane

The fluoride removal mechanism is essential for understanding the membrane's efficacy. Even though the membrane itself is negatively charged, which would normally repel anions like fluoride ions, the incorporation of activated clay and bauxite into the PVA matrix brings additional functionalities, thus enabling effective fluoride rejection.[52]

Fluoride removal is fundamentally based on the adsorption characteristics of the embedded activated clay and bauxite.[53] These materials present large surface areas, which are instrumental in attracting and binding fluoride ions. The highly layered structure of activated clay with an enormous specific surface area presents various sites for fluoride ion adsorption. Similarly, bauxite, as an aluminium-rich material, can exert an electrostatic attraction with fluoride ions.[54] The bauxite component may also promote ion exchange processes.[55]

In context, fluoride ions in the water can displace other anions such as hydroxide (OH$^-$), sulphate (SO$_4^{2-}$), bicarbonate (HCO$_3^-$), and chloride (Cl$^-$) from the active sites that are weakly bound within bauxite.[56] This ion exchange activity pre-

Table 5 Comparison of our membrane's efficiency to other membranes

Membrane	Flux (L m^{-2} h^{-1})	Removal efficiency (%)	Ion removed	Reference
PSf/bentonite	46.0	59.2	Cu(II) ion	(Abd Hamid et al., 2020[25])
PSf/zeolite	126.0	97.0	Cu(II) ion	(Abd Hamid et al., 2020[25])
GCTACC/PAN	5.6	65.0	Na$_2$SO$_4$	(Huang et al., 2006[50])
SCS/PAN	7.9	41.5	MgSO$_4$	(Miao et al., 2005[51])
SCS/PAN	11.3	92.8	K$_2$SO$_4$	(Miao et al., 2005[51])
MPVA/1BXT:2AC	73.1	82.6	F$^-$ ion	Present work

vails with its greatest efficacy in areas where the competing anions are not significantly abundant; therefore, fluoride ions will most likely occupy the exchange sites in such specific environments.[57] There is an aspect of great importance when it comes to fluoride removal, which is the realization of possible complexation reactions.[45] Some metal oxides like aluminium oxide (Al_2O_3), iron oxide (Fe_2O_3), titanium dioxide (TiO_2), and silicon dioxide (SiO_2), or hydroxides in bauxite, can exhibit interaction with fluoride for the formation of stable products.[58] These compounds will not be so easily rejected through the negatively charged membrane matrix, enabling fluoride to remain within the membrane structure. Aluminium ions in bauxite can produce aluminium–fluoride complexes, which are efficiently immobilized in the membrane.

The antifouling properties of membranes are further relevant in ensuring the long-term performance of fluoride removal. The embedded activated clay and bauxite prevent any organic and inorganic foulants from blocking the active sites, making the membrane less effective in adsorbing fluoride. Hence, by controlling fouling, the membrane ensures the accessibility of its active sites for continuous and efficient removal of fluoride.

4. Conclusion

This study aimed at fabricating PVA-based composite membranes using different ratios of bauxite (BXT) and activated clay (AC) as fillers to reduce membrane fouling in water defluorination. Membranes were fabricated through the solution casting method and extensively characterized using FTIR, XRD, ^{1}H NMR, SEM/EDS, and zeta-potential analyses. FTIR and ^{1}H NMR confirmed the chemical interactions and bonding between PVA and fillers, and XRD gave insights into the crystalline phases, structural orientation, and crystallinity of membranes. SEM/EDS revealed a comprehensive insight into the membrane's surface and elemental compositions. The incorporation of BXT and AC improved the physical properties of the membrane by enhancing porosity, mechanical strength, hydrophilicity, and permeability. With a water flux of 73.1 L m^{-2} h^{-1}, a porosity of 69.2%, a fluoride removal efficiency of 92.4%, and an antifouling efficiency of 82.6%, the best performance was seen with the MPVA/1BXT:2AC membrane. These results indicate the function of hydrophilic functional groups in BXT and AC to minimize foulant accumulation and efficiently enhance membrane performance for water treatment applications.

Conflicts of interest

The authors declare no conflicts of interest concerning the publication of this paper.

Data accessibility

The data used in this research article were gathered from our experiment. Supporting data for the results of this study are included in the article and will be made available upon request from the corresponding author.

Ethical statement

This article does not address analysis with ethical concerns.

Data availability

The data supporting the findings of this study are available from the corresponding author upon reasonable request. All relevant experimental data, including membrane characterization results, defluorination performance, and water quality analysis, have been included in the manuscript.

Acknowledgements

References

1 N. Akhtar, M. I. Syakir Ishak, S. A. Bhawani and K. Umar, Various natural and anthropogenic factors responsible for water quality degradation: A review, *Water*, 2021, **13**(19), 2660.

2 I. Mukherjee and U. K. Singh, Groundwater fluoride contamination, probable release, and containment mechanisms: a review on Indian context, *Environ. Geochem. Health*, 2018, **40**(6), 2259–2301.

3 J. Patel, H. G. Gosai, S. Mujumdar and V. K. Srivastava, Fluoride and Fluorocarbon in Soil and Plant: Sources, Toxicity, and Prevention Methods, in *Fluoride and Fluorocarbon Toxicity: Sources, Issues, and Remediation*, Springer Nature Singapore, Singapore, 2024, pp. 345–366.

4 Z. Ullah, A. Rashid, J. Nawab, A. U. Bacha, J. Ghani, J. Iqbal, Z. Zhu, A. F. Alrefaei and M. H. Almutairi, Fluoride contamination in groundwater of community tube wells, source distribution, associated health risk exposure, and suitability analysis for drinking from arid zone, *Water*, 2023, **15**(21), 3740.

5 N. Singh, A. Dhillon and D. Kumar, Metal-organic frameworks for adsorption of fluoride for groundwater treatment, *Groundwater Sustainable Dev.*, 2023, **23**, 100967.

6 P. Grandjean, Developmental fluoride neurotoxicity: an updated review, *Environ. Health*, 2019, **18**(1), 110.

7 G. W. Ashong, B. A. Ababio, E. E. Kwaansa-Ansah, S. K. Koranteng and G. D. Muktar, Investigation of fluoride concentrations, water quality, and non-carcinogenic health

risks of borehole water in bongo district, northern Ghana, *Heliyon*, 2024, **10**(6), 1–11.

8 L. Craig, A. Lutz, K. A. Berry and W. Yang, Recommendations for fluoride limits in drinking water based on estimated daily fluoride intake in the Upper East Region, Ghana, *Sci. Total Environ.*, 2015, **532**, 127–137.

9 E. D. Sunkari, S. J. Adams, M. B. Okyere and P. Bhattacharya, Groundwater fluoride contamination in Ghana and the associated human health risks: any sustainable mitigation measures to curtail the long term hazards?, *Groundwater Sustainable Dev.*, 2022, **16**, 100715.

10 E. D. Sunkari, M. S. Zango and H. M. Korboe, Comparative analysis of fluoride concentrations in groundwaters in northern and southern Ghana: implications for the contaminant sources, *Earth Syst. Environ.*, 2018, **2**(1), 103–117.

11 Y. S. Solanki, M. Agarwal, A. B. Gupta, S. Gupta and P. Shukla, Fluoride occurrences, health problems, detection, and remediation methods for drinking water: A comprehensive review, *Sci. Total Environ.*, 2022, **807**, 150601.

12 A. Dongzagla, S. Jewitt and S. O'Hara, Assessment of fluoride concentrations in drinking water sources in the Jirapa and Kassena-Nankana Municipalities of Ghana, *Groundwater Sustainable Dev.*, 2019, **9**, 100272.

13 F. Damiri, S. Andra, N. Kommineni, S. K. Balu, R. Bulusu, A. A. Boseila, D. O. Akamo, Z. Ahmad, F. S. Khan, M. H. Rahman and M. Berrada, Recent advances in adsorptive nanocomposite membranes for heavy metals ion removal from contaminated water: a comprehensive review, *Materials*, 2022, **15**(15), 5392.

14 R. Ben Dassi and B. Chamam, Nanomaterial-enhanced membranes for advanced water and wastewater treatment: a comprehensive review, *Rev. Environ. Sci. Bio/Technol.*, 2025, 1–35.

15 P. Su, S. Chen, L. Chen and W. Li, Constructing polymer/metal-organic framework nanohybrids to design compatible polymer-filler-polymer membranes for CO2 separation, *J. Membr. Sci.*, 2024, **691**, 122246.

16 C. A. Crock, A. R. Rogensues, W. Shan and V. V. Tarabara, Polymer nanocomposites with graphene-based hierarchical fillers as materials for multifunctional water treatment membranes, *Water Res.*, 2013, **47**(12), 3984–3996.

17 M. Zahid, A. Rashid, S. Akram, Z. A. Rehan and W. J. Razzaq, A comprehensive review on polymeric nanocomposite membranes for water treatment, *J. Membr. Sci. Technol.*, 2018, **8**(1), 1–20.

18 A. A. Sapalidis, Porous polyvinyl alcohol membranes: preparation methods and applications, *Symmetry*, 2020, **12**(6), 960.

19 N. M. Zainudeen, L. Mohammed, A. Nyamful, D. Adotey and S. K. Osae, A comparative review of the mineralogical and chemical composition of African major bauxite deposits, *Heliyon*, 2023, **9**(8), 1–22.

20 E. I. Unuabonah, C. Günter, J. Weber, S. Lubahn and A. Taubert, Hybrid clay: a new highly efficient adsorbent for water treatment, *ACS Sustainable Chem. Eng.*, 2013, **1**(8), 966–973.

21 S. I. Alhassan, L. Huang, Y. He, L. Yan, B. Wu and H. Wang, Fluoride removal from water using alumina and aluminum-based composites: A comprehensive review of progress, *Crit. Rev. Environ. Sci. Technol.*, 2021, **51**(18), 2051–2085.

22 C. Liu, X. Lu, J. Gu, C. Wu, S. Zheng and Z. Liu, Preparation of high-flux membrane for dye desalination by the stacked swelling strategy of small-molecule side chains, *J. Membr. Sci.*, 2024, **709**, 123075.

23 Y. Qiu, L. F. Ren, J. Shao, L. Xia and Y. Zhao, An integrated separation technology for high fluoride-containing wastewater treatment: Fluoride removal, membrane fouling behavior and control, *J. Cleaner Prod.*, 2022, **349**, 131225.

24 K. Wang, S. Wang, K. Gu, W. Yan, Y. Zhou and C. Gao, Ultra-low pressure PES ultrafiltration membrane with high-flux and enhanced anti-oil-fouling properties prepared via *in situ* polycondensation of polyamic acid, *Sci. Total Environ.*, 2022, **842**, 156661.

25 S. Abd Hamid, M. Shahadat, B. Ballinger, S. F. Azha, S. Ismail, S. W. Ali and S. Z. Ahammad, Role of clay-based membrane for removal of copper from aqueous solution, *J. Saudi Chem. Soc.*, 2020, **24**(10), 785–798.

26 M. K. Alsebaeai, A. L. Ahmad and B. S. Ooi, Construction of wetting resistance surface of highly hydrophobic PVDF-HFP/rGO coated supported PVDF hollow fiber composite membrane for membrane distillation, *Chem. Eng. J.*, 2024, **493**, 152565.

27 S. Li, R. Zhang, J. Xie, D. E. Sameen, S. Ahmed, J. Dai, W. Qin, S. Li and Y. Liu, Electrospun antibacterial poly (vinyl alcohol)/Ag nanoparticles membrane grafted with 3, 3′, 4, 4′-benzophenone tetracarboxylic acid for efficient air filtration, *Appl. Surf. Sci.*, 2020, **533**, 147516.

28 C. Kina. Sustainable cement-based materials blended with recycled water treatment sludge and other various waste products as binder: Characterization and environmental-economical impacts.

29 P. Castaldi, M. Silvetti, S. Enzo and P. Melis, Study of sorption processes and FT-IR analysis of arsenate sorbed onto red muds (a bauxite ore processing waste), *J. Hazard. Mater.*, 2010, **175**(1–3), 172–178.

30 A. A. Oduro, S. A. Biney, E. S. Nortey, A. Kangmennaa, R. B. Forkuo and E. S. Agorku, Polyvinyl alcohol embedded activated clay/hydroxyapatite membranes for fouling control during the removal of an organic dye in water, *J. Appl. Polym. Sci.*, 2025, **142**(14), e56701.

31 S. Belfer, R. Fainchtain, Y. Purinson and O. Kedem, Surface characterization by FTIR-ATR spectroscopy of polyethersulfone membranes-unmodified, modified and protein fouled, *J. Membr. Sci.*, 2000, **172**(1–2), 113–124.

32 G. U. Alaneme, K. A. Olonade and E. Esenogho, Eco-friendly agro-waste based geopolymer-concrete: A systematic review, *Discover Mater.*, 2023, **3**(1), 14.

33 M. Liaqat, *Development of Biodegradable Flame Retardant Polymer Nanocomposites*, Doctoral dissertation, Chemistry Department COMSATS University Islamabad, Lahore Campus, 2024.

© 2025 The Author(s). Published by the Royal Society of Chemistry

RSC Appl. Polym., 2025, **3**, 1613–1628 | **1627**

34 S. Mallapragada, *Molecular analysis and experimental investigation of the dissolution mechanism of semicrystalline polymers*, Doctoral dissertation, Purdue University, 1996.

35 S. Yang, Y. Huang, Q. Wang, J. Deng, X. Liu and J. Wang, Mineralogical and geochemical features of karst bauxites from Poci (western Henan, China), implications for parental affinity and bauxitization, *Ore Geol. Rev.*, 2019, **105**, 295–309.

36 Y. Kazemi, A. R. Kakroodi, L. H. Mark, T. Filleter and C. B. Park, Effects of polymer-filler interactions on controlling the conductive network formation in polyamide 6/multi-Walled carbon nanotube composites, *Polymer*, 2019, **178**, 121684.

37 M. Doumeng, F. Berthet, K. Delbé, O. Marsan, J. Denape and F. Chabert, Effect of size, concentration, and nature of fillers on crystallinity, thermal, and mechanical properties of polyetheretherketone composites, *J. Appl. Polym. Sci.*, 2022, **139**(5), 51574.

38 O. S. Lezova, D. V. Myasnikov, O. A. Shilova, A. G. Ivanova and S. I. Selivanov, Study of the composition and structure of ion-conducting membranes based on polyvinyl alcohol by ^{1}H NMR spectroscopy, *Int. J. Hydrogen Energy*, 2022, **47**(7), 4846–4853.

39 S. Moulay, Poly (vinyl alcohol) functionalizations and applications, *Polym.-Plast. Technol. Eng.*, 2015, **54**(12), 1289–1319.

40 S. B. Aziz, M. M. Nofal, H. O. Ghareeb, E. M. Dannoun, S. A. Hussen, J. M. Hadi, K. K. Ahmed and A. M. Hussein, Characteristics of poly (Vinyl alcohol)(PVA) based composites integrated with green synthesized Al3+-metal complex: Structural, optical, and localized density of state analysis, *Polymers*, 2021, **13**(8), 1316.

41 V. Dharini, S. P. Selvam, J. Jayaramudu and R. S. Emmanuel, Functional properties of clay nanofillers used in the biopolymer-based composite films for active food packaging applications-Review, *Appl. Clay Sci.*, 2022, **226**, 106555.

42 S. Y. Lee and R. J. Gilkes, Groundwater geochemistry and composition of hardpans in southwestern Australian regolith, *Geoderma*, 2005, **126**(1–2), 59–84.

43 J. K. Adusei, E. S. Agorku, R. B. Voegborlo, F. K. Ampong, B. Y. Danu and F. A. Amarh, Removal of Methyl red in aqueous systems using synthesized NaAlg-g-CHIT/nZVI adsorbent, *Sci. Afr.*, 2022, **17**, e01273.

44 Y. Guo, Y. Zhao, S. Wang, C. Jiang and J. Zhang, Relationship between the zeta potential and the chemical agglomeration efficiency of fine particles in flue gas during coal combustion, *Fuel*, 2018, **215**, 756–765.

45 Z. Zeng, Q. Li, J. Yan, L. Huang, S. R. Arulmani, H. Zhang, S. Xie and W. Sio, The model and mechanism of adsorptive technologies for wastewater containing fluoride: a review, *Chemosphere*, 2023, **340**, 139808.

46 W. Lu, C. Zhang, Y. Du, B. Quan, Z. Qin, K. Cheng, A. Niyazi and P. Su, Applications of nanoadsorbents for the removal of fluoride from water: Recent advancements and future perspectives, *Sep. Purif. Rev.*, 2024, **53**(3), 311–335.

47 R. Ryskulov, E. Pedrueza-Villalmanzo, Y. A. Tatli, I. Gözen and A. Jesorka, Complete de-wetting of lipid membranes on silicon carbide, *Eur. Phys. J.: Spec. Top.*, 2024, **233**(17), 2743–2756.

48 A. Abdelrasoul, H. Doan, A. Lohi and C. H. Cheng, Modeling of fouling and fouling attachments as a function of the zeta potential of heterogeneous membrane surfaces in ultrafiltration of latex solution, *Ind. Eng. Chem. Res.*, 2014, **53**(23), 9897–9908.

49 K. A. Alfredo. Drinking water treatment by alum coagulation: competition among fluoride, natural organic matter, and aluminum.

50 R. Huang, G. Chen, M. Sun and C. Gao, A novel composite nanofiltration (NF) membrane prepared from graft copolymer of trimethylallyl ammonium chloride onto chitosan (GCTACC)/poly (acrylonitrile)(PAN) by epichlorohydrin cross-linking, *Carbohydr. Res.*, 2006, **341**(17), 2777–2784.

51 J. Miao, G. H. Chen and G. J. Gao, A novel kind of amphoteric composite nanofiltration membrane prepared from sulfated chitosan (SCS), *Desalination*, 2005, **181**(1–3), 173–183.

52 V. Gitis and G. Rothenberg, *Ceramic membranes: new opportunities and practical applications*, John Wiley & Sons, 2016.

53 A. Dhillon, S. Prasad and D. Kumar, Recent advances and spectroscopic perspectives in fluoride removal, *Appl. Spectrosc. Rev.*, 2017, **52**(3), 175–230.

54 Y. Li, Y. Yang, G. Qu, Y. Ren, Z. Wang, P. Ning, F. Wu and X. Chen, Reuse of secondary aluminum ash: Study on removal of fluoride from industrial wastewater by mesoporous alumina modified with citric acid, *Environ. Technol. Innovation*, 2022, **28**, 102868.

55 Y. Zhang, Q. Shi, M. Luo, H. Wang, X. Qi, C. H. Hou, F. Li, Z. Ai and J. T. Junior, Improved bauxite residue dealkalization by combination of aerated washing and electrodialysis, *J. Hazard. Mater.*, 2019, **364**, 682–690.

56 B. Al Sabti, D. R. Samayamanthula, F. M. Dashti and C. Sabarathinam, Fluoride in groundwater: distribution, sources, processes, analysis, and treatment techniques: a review, in *Hydrogeochemistry of Aquatic Ecosystems*, 2023, pp. 1–31.

57 A. Bhatnagar, E. Kumar and M. Sillanpää, Fluoride removal from water by adsorption—a review, *Chem. Eng. J.*, 2011, **171**(3), 811–840.

58 N. J. Ismail, *Metal oxides incorporated bauxite hollow fibre photocatalytic membrane for bisphenol a removal from aqueous solution*, Doctoral dissertation, Universiti Teknologi, Malaysia, 2022.